Available online at www.sciencedirect.com

ScienceDirect

Ceramics International 40 (2014) 1461–1470

CERAMICS INTERNATIONAL

www.elsevier.com/locate/ceramint

Superconducting properties of polycrystalline $YBa_2Cu_3O_{7-d}$ prepared by sintering of ball-milled precursor powder

A. Hamrita[a], Y. Slimani[a], M.K. Ben Salem[a], E. Hannachi[a], L. Bessais[b], F. Ben Azzouz[a], M. Ben Salem[a,*]

[a]*L3M, Department of Physics, Faculty of Sciences of Bizerte, University of Carthage, 7021 Zarzouna, Tunisia*
[b]*CNRS-ICMPE-UMR 7182 University, Paris 12, France*

Received 6 May 2013; received in revised form 26 June 2013; accepted 4 July 2013
Available online 12 July 2013

Abstract

The effect of ball milling on the superconducting properties of polycrystalline $YBa_2Cu_3O_y$ compounds has ben studied. The samples were synthesized by a solid state reaction by considering a thermal cycle with two stages of sintering at 950 °C separated by intermediate crushing; a traditional crushing (in a mortar) and another energetic (in a planetary crusher). The correlations between milling parameters, microstructure and superconducting properties have been investigated. The samples were characterized by X-ray diffraction, energy dispersive spectrometry and scanning electron microscopy. The critical current density of the samples was examined using current–voltage, ac-susceptibility and magnetization measurements. The temperature dependence of the resistivity under magnetic field has been studied to evaluate the upper critical and the irreversibility magnetic fields of these samples. It is demonstrated that ball milling is an effective approach for obtaining fine particles with size about 15 nm gathered into coral-like agglomerates and embedded in the matrix. Such decorated finer structure contributes to the enhancement of the inter-grains and intra-grains critical current density of the material under an applied magnetic field.
Published by Elsevier Ltd

Keywords: B. Structure; C. Electrical properties; Flux pinning; Planetary ball milling; YBCO superconductor

1. Introduction

For most applications of high temperature superconductor (HTS) materials a high critical current density J_c under magnetic field is required. For polycrystalline samples, the inter-granular critical current density is limited by weak links caused by grains boundaries and the intra-granular critical current is impeded principally by the thermally activated flux flow at high temperatures and the applied magnetic field. To prevent the vortex motions and enhance the flux pinning strength it is necessary to introduce artificial pinning centers in the superconductor, apart from those which occur naturally [1]. Crystal imperfections such as-low-angle grain boundaries, stacking faults, oxygen vacancies twin boundaries, impurity phases precipitates, poor superconducting phase and dislocations can act as potential pinning centers [2–8]. The route of artificially introducing inhomogeneities or second-phase materials as flux pinning sites in the processing of bulk $YBa_2Cu_3O_7$ (Y-123 or YBCO for brevity) is a long standing topic. Such artificial pinning centers can be generated in the YBCO material by adding the respective oxides during the first thermal cycle, by adding previously prepared, fully reacted second-phase materials to the precursor powder or by precipitation from a single phase superconductor [4,5]. Various techniques have been reported in the literature to increase the density of these defects [9,10]. However, different fabrication processes can result in different intermediate phases in equilibrium and consequently affect the microstructure development and the superconducting properties in polycrystalline YBCO. Recently, mechanical milling has been proved to be an effective technique for raising the flux pinning properties in the case of MgB_2 [11–18]. The influence of high-energy milling on the superconducting properties of some chemical doped MgB_2 bulk samples, tapes and wires has also been reported in the literature [14–18].

For the Y-based compound, high energy ball milling has been used to produce nanocrystalline $YBa_2Cu_3O_{7-d}$ powders [19,20]. It is reported that after about 1 h of milling a transition

*Corresponding author. Tel.: +216 72 591 906; fax: +216 72 590 566.
E-mail addresses: salemwiem2005@yahoo.fr, mohamed.bensalem@fsb.rnu.tn (M. Ben Salem).

0272-8842/$ - see front matter Published by Elsevier Ltd
http://dx.doi.org/10.1016/j.ceramint.2013.07.030

from orthorhombic to tetragonal and finally to a cubic metastable phase has been observed with a total loss of superconductivity. However, when the nanocrystalline phase was subjected to a high-temperature heat treatment the tetragonal structure is produced. Recently, we have studied the effect of planetary milling in YBCO compounds [21,22]. The YBCO bulk is prepared using planetary ball milling and a subsequent sintering at 950 °C. We reported that the planetary milled ceramics for 4 h with a ball to powder ratio 5:1 and speed rotation 600 rpm possess a large magneto-resistance in weak magnetic fields over a wide temperature range including liquid nitrogen temperature compared to the unmilled ceramic [21]. The use of the planetary ball milling technique allows us to obtain a sensitive electrical response of the superconductor to a weak magnetic field. Little attention is paid to the role of the microstructural development with respect to the improvement of the superconducting properties of YBCO processed using ball milling. We have studied the effect of silver inclusions on the superconducting properties of $YBa_2Cu_3O_y$ prepared using planetary ball milling and we have shown that the better pinning properties of the Ag-added milled samples are believed to be due to the microstructure of more finely and uniformly distributed silver and Y-deficient nanosized generated by ball milling [22]. In the present work we evaluate the transport and pinning properties of $YBa_2Cu_3O_{7-d}$ ceramics derived from the sintered milled powders.

2. Experimental process

Polycrystalline samples of $YBa_2Cu_3O_y$ were synthesized by solid state reaction. Commercially available powders Ba_2CO_3 (purity $>99\%$) Y_2O_3 (99.99%purity), and CuO (purity $>99.3\%$) were used as starting materials. The starting powders were mixed according to the chemical formula of Y:Ba:Cu = 1:2:3 by hand grinding in an agate mortar with an agate pestle. This mixture of powders was pelletized and then calcined at 950 °C for 12 h in air in order to produce an oxide precursor without remainder of any carbonates. The resulting oxide precursor was divided into two parts: one part was ground by hand in an agate mortar with an agate pestle, the second part of the oxide precursor was milled via the planetary milling technique and another was ground by hand. Ball-milling facilitates the formation of a homogeneous compound with an optimal microstructure characterized by a high grain boundary density and lattice strain, which is expected to enhance the magnetic flux pinning ability and to improve the critical currents of superconductor materials in an external magnetic field. This technique involves the optimization of a number of variables as ball-to-powder weight ratio, speed rotation and number of balls to achieve a desired microstructure for critical current density and pinning properties enhancement. The mechanical milling of the oxide precursor was performed in air, using a Retsch PM 200F planetary ball mill with vial and balls of stainless steel. The ball-milling was carried out for 4 h and the milling was stopped for 5 min every 25 min in order to cool down the system. Two milling rotation speeds were set at 600 rpm and 400 rpm with various ball-to-powder weight ratio and 5 g of oxide precursor is usually placed into the container. In Table 1 we summarized the experimental data for the milled samples. Both milled and hand grinded oxide precursors were then pressed uniaxially into pellets of 0.5 mm thick and 7 mm in diameter under a pressure of 750 MPa. These pellets were sintered in air at 950 °C for 8 h and then furnace cooled to room temperature. The samples prepared using ball-milling and hand grinding are referred to as "milled" and "unmilled" samples in the following text.

The structure and the phase purity were examined by powder X-ray diffraction (XRD) using a Philips 1710 diffractometer with CuK_α radiation. The scanning electron microscope (SEM) measurements were performed using an FEI Nano Lab 200. Chemical analysis was performed using the energy dispersive X-ray spectroscopy (EDXS) system attached to the SEM. The transport properties of the samples were studied by measuring the electrical resistivity–temperature $\rho(T)$and current–voltage (I–V) characteristics using the four-probe technique. The pellets were carefully cut into bar shaped samples with almost similar dimensions. Electrical contacts were made using silver paint and the contact resistance value was approximately0.5 Ω. The temperature dependence of the electrical resistivity $\rho(T,H)$ under applied magnetic fields ranging from 0 to 7 T was measured. The magnitude of the excitation current density, J, used to measure the resistivity of the samples is$J = 40\ \mu A\ cm^{-2}$. The isothermal magnetization (M–H) of the samples was measured by using a Quantum Design Physical Properties Measurement System (PPMS9) at 77 K in magnetic fields up to 6 T. The sample was mounted such as that its wide surface was along the direction of the magnetic field. We have also explored the AC-magnetic

Table 1
Notations, experimental conditions and phase compositions of the unmilled and milled samples.

Sample notation	Ball-milling			Phase compositions (vol%)		
	Rotation speed	Ball-to weight ratio powder	Number of balls	Y-123	Y-deficient 123	Secondary phase
A-milled	600	10:1	4	62.8	30.4	6.8
B-milled	600	5:1	4	79.7	18.1	2.2
C-milled	600	5:2	3	91.3	8.1	0.6
D-milled	400	5:2	3	95.00	4.5	0.5
Unmilled	Hand grinding			99.5	0	0.5

properties of the samples by measuring the in-phase and out of-phase components of their AC susceptibilities. AC-susceptibility apparatus was also the PPMS9, and the measurements were carried out in a field ranging from 1 to 10 Oe at the frequency of 1000 Hz. The transport critical current density (J_{ct}) values were determined at various temperatures using a 5 μV/cm criterion and a magnetic field was applied along the short axis of the samples and the excitation current was injected along the length axis of the samples. The magnetic critical current density, $J_{cm}(H)$, values determined from the hysteresis width of the magnetization measurements were estimated according to the extended Bean model [23–25] by using the following equation:$J_{cm} = 20(\Delta M)/a(1-a/3b)$, where a and b are the cross-sectional dimensions of the sample perpendicular to the applied field.

3. Results and discussion

Fig. 1 shows the XRD patterns of the milled and unmilled samples sintered at 950 °C. The XRD analysis shows that all samples are mainly composed of perovskite based Y-123 with orthorhombic Pmmm symmetry with small quantities of Y_2BaCuO_5 and $BaCuO_2$ as secondary phases. The XRD data have been analyzed by the Rietveld refinement procedure using the FULLPROF program with multiphase capability and pseudo-Voight peak shape functions. The R_p and R_{wp} factors and the goodness of fit χ^2 were used as the numerical criteria of fitting. The Rietveld method was successfully applied to determine quantitatively phase abundances of the different crystallographic phases in the compound. This methodology considers simultaneously all reflections of all phases irrespective of reflections are overlapping or well resolved, and provide a very accurate result of the structural and microstructural parameters. SEM observations and EDXS analyses (see Figs. 2–4) show that the milled samples exhibit nanoscale entities of Y-deficient YBCO submerged within the Y-123 crystallites. Therefore a fitting of the XRD data of ball milled samples was tried considering stoichiometric Y-123, Y-deficient YBCO and secondary phases such as (Y-124 and Y-211). The estimated concentrations of the different phases are given in Table 2. It is clear that the concentration of phases depends on the history of the grinding. The Y-deficient YBCO phase concentration is increased from 4.5 to 30.4 wt% with increasing the ball to powder weight ratio and the speed of rotation. The A-milled sample elaborated with a ball-to-powder weight ratio 10:1 and a speed rotation of 600 rpm exhibits a large quantity of Y-deficient YBCO and secondary phases.

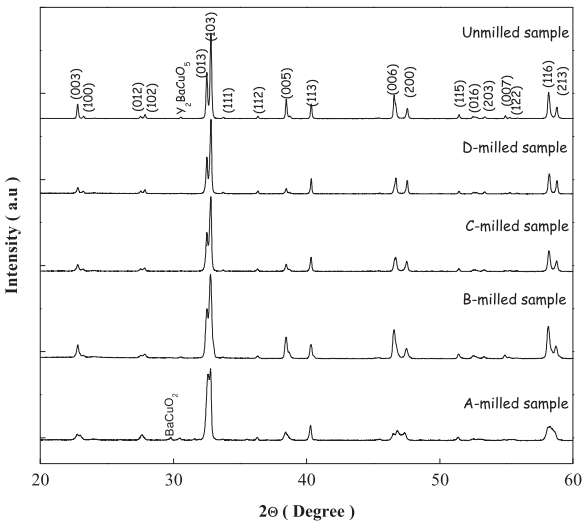

Fig. 1. X-ray powder diffraction patterns of the unmilled and milled samples.

The SEM micrographs of the transverse cross-section morphology at different magnifications of the sintered samples derived from YBCO precursor oxide with and without ball milling are shown in Fig. 2. The microstructure exhibits a morphology with faceted grains of $YBa_2Cu_3O_y$ randomly oriented. This indicates that grain growth has occurred during sintering of the milled precursor oxide. A good connectivity between grains and relatively dense packing is present in all samples. The C-milled sample exhibits a smaller grain size when compared to the other samples. High magnification images (right part of Fig. 2) of the milled samples show the presence of spherical shape entities bright in contrast. These entities are visible inside the grains along with some segregation at the grain boundaries. Such entities have not been observed in unmilled samples. The density of these entities increases when increasing the weight ball proportion and rotation speed. This result is consistent with the XRD analysis. A closer look at higher magnification (Fig. 3a, b) reveals that the spherical shape entities appear as a clumping of fine particles with a particle size of about 15 nm into coral-like agglomerates. This result is in good agreement with the XRD evaluation using the well known Scherrer equation; the estimated average crystallite size is about 20 nm. The finer grains structure embedded in the superconductor would bring about more disorder and fine scale lattice defects in the grain boundary region and can result in an increase of vortex pinning centers and subsequently enhances the pinning properties of the samples. The EDXS resolution in the SEM is about 1–2 μm, so it is impossible to determine precisely the composition of the entities by conducting a spot analysis on a single particle. To estimate the elemental composition of the entities, comparative analyses have been carried out in the regions where entities are present and regions where they are absent. For the milled sample the EDXS analysis performed on areas with a high-density of entities shows the presence of Y, Ba, Cu, and O with a small deviation of the yttrium content compared to the nominal composition of $YBa_2Cu_3O_y$ (Fig. 4). The chemical composition is illustrated in the inset of Fig. 4. In the quantitative analyses we have omitted the oxygen but we can estimate the cation proportions of Y/Ba/Cu.

Fig. 5 shows the temperature dependence of the normalized electrical resistivity$\rho(T)/\rho(285\ K)$ ($\rho(285\ K)$ is the room temperature resistivity) for both samples. Note that the unmilled sample shows a one-step transition at$T_c^{onset} = 92$ K. However for the milled samples the $\rho(T)$ measurements indicate two rapid resistivity drops. The second drop is accentuated by increasing the ball-to-powder weight ratio and the rotation speed. Some studies have been used to support the contention that the double transition is an intrinsic property of the YBCO superconductor order parameter, whereas others attribute this effect to phase separation in

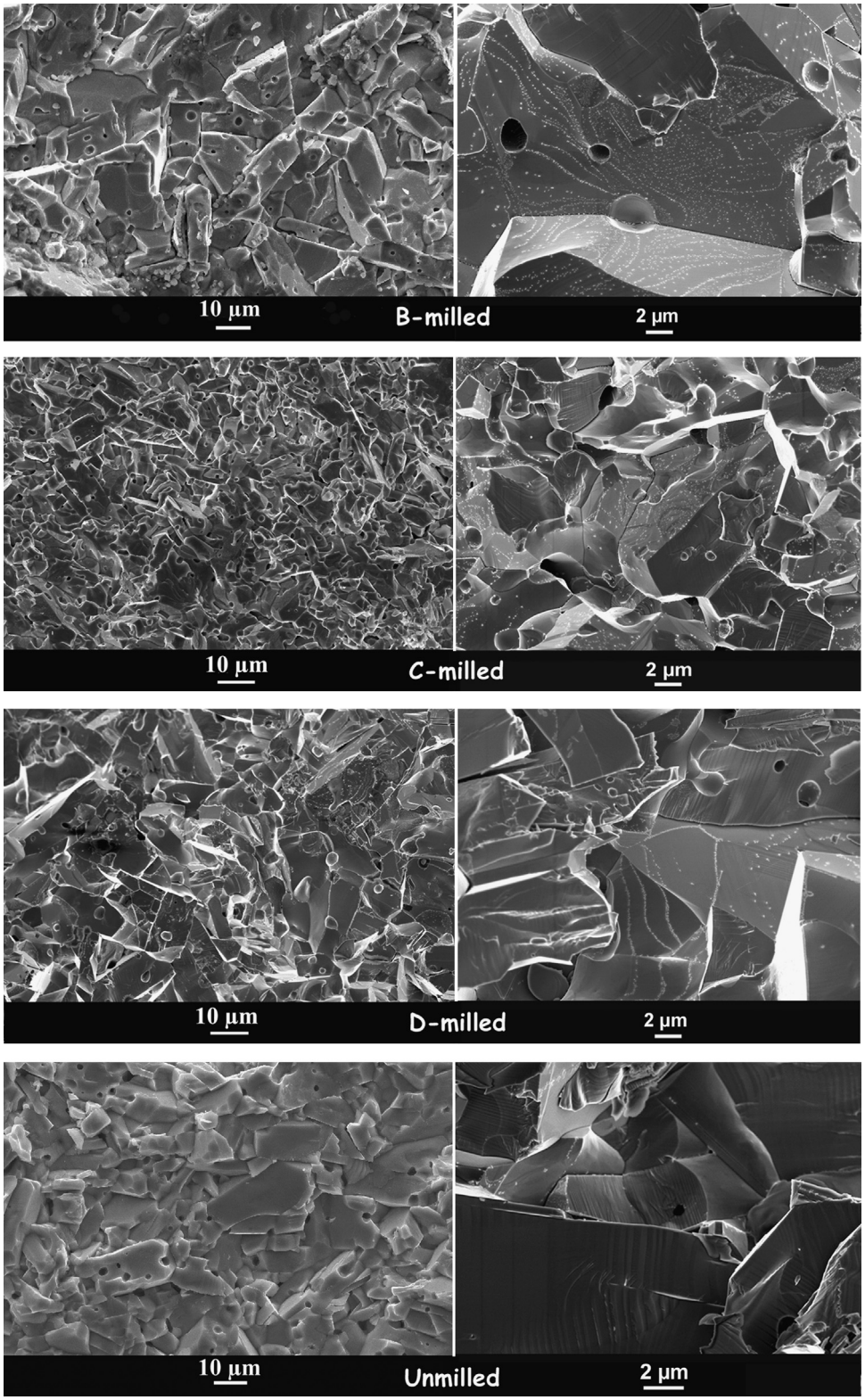

Fig. 2. SEM micrographs of the unmilled and milled samples. Low magnification (left) and high magnification (right).

YBCO at different doping levels [26]. XRD and SEM analyses indicate the presence of both Y-123 and Y-deficient YBCO phases in the milled samples, thus the observation of a double superconducting transition suggests that the first transition arises from the $YBa_2Cu_3O_{7-d}$ phase while the second results from aY-deficient YBCO phase. The A-milled sample has a lower zero resistance temperature,T_{co}, of 66 K and a broader superconducting transition of 17 K. It is well established that using hard conditions of mechanical milling result in a decrease of the T_{co} (Table 2) with larger transition width

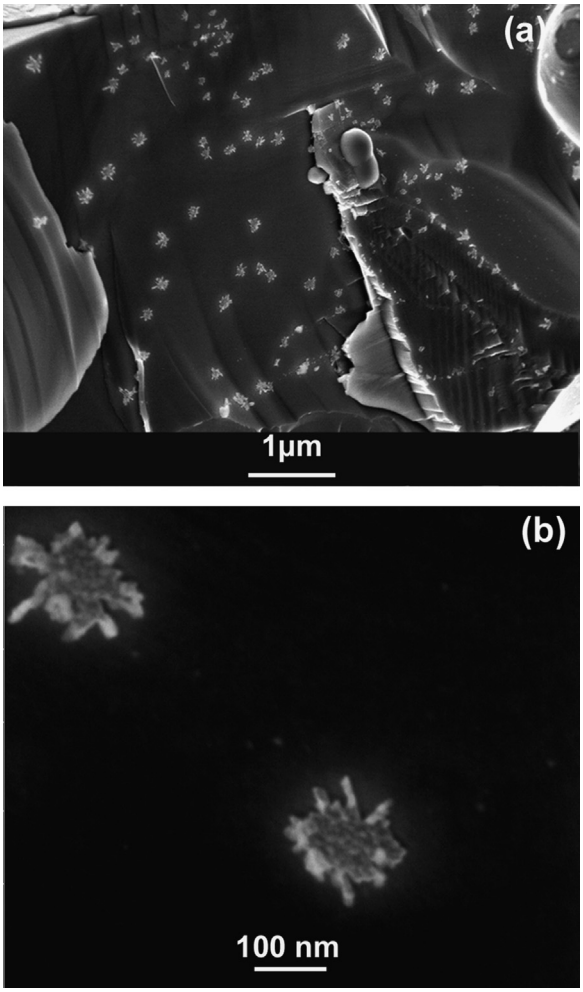

Fig. 3. High magnification SEM micrographs showing nanosized particles within Y-123.

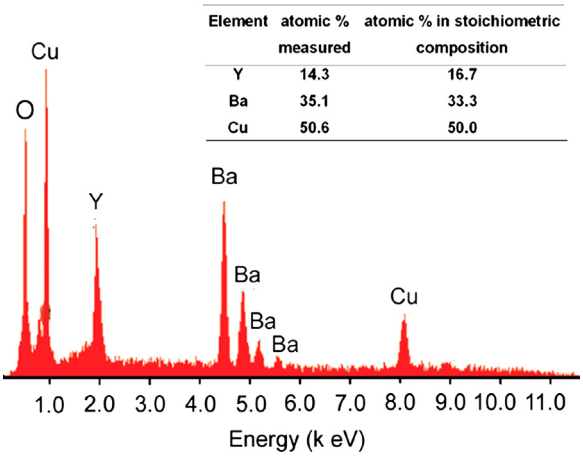

Fig. 4. EDXS spectrum taken from the area with high-density of nanoscale entities. Inset: quantitative chemical composition.

implying a significant perturbation of the microstructure in these samples caused by either interfaces, heterogeneities or induced defects. The larger the number of defects, heterogeneities etc, the higher their scattering offered to the mobile carriers. This is confirmed by the higher residual resistivity $\rho_n(0)$values for milled samples.

In order to estimate the values of the upper critical $H_{c2}(T)$ and irreversibility $H_{irr}(T)$ magnetic fields of the samples we measured the magnetic field dependence of the resistivity versus temperature $\rho\,(T,\,H)$. The temperature dependence of the resistivity ($\rho\,(T,\,H)$) under applied magnetic fields ranging from 0 to 7 T are measured (Fig. 6). The $\rho\,(T,\,H)$ transition curves are characterized by two distinct sections; the upper region (steep part) characterizes the intragranular transition and the lower region characterizes the grain-boundaries network or intergranular effects, which are considered to be weak Josephson type links. With the application of a magnetic field, the steep part slowly shifts towards the lower temperatures while the tail part shifts at a faster rate.

The irreversibility temperature(T_{irr})is decided by the weak links between grains as well as by the vortex motion flow of the magnetic flux lines. The $T_{irr}(H)$ values are taken at $\rho = 0.01\ \rho_n$ whereρ_n is the normal state resistivity before the superconducting transition. Fig. 7a shows the irreversibility field $\mu_o H_{irr}$ of unmilled and C-milled samples. The magnetic irreversibility as a function of temperature is usually fitted by the $H_{irr}(t) = H_{irr}(0)\ (1-t)^n$ equation predicted by the collective pinning theory [27], with $t = T_{irr}\ (H)/T_{irr}(0)$ and $H_{irr}(0)$, $T_{irr}(0)$ and n are fitting parameters. The obtained fitting constants for the unmilled sample are $\mu_o H_{irr}(0) = 16\ T$and $n = 1.57 \pm 0.03$ while for the C-milled sample they are $\mu_o H_{irr}(0) = 21\ T$ and $n = 1.85 \pm 0.03$. These results show that for the unmilled sample $H_{irr}(T)$can be well fitted by the giant-flux creep line while the C-milled sample data are represented by vortex melting line [28].

Different criteria of determining the upper critical magnetic field, $H_{c2}(T)$, have been reported in the literature [29–31]. The estimation of the temperature dependence of the resistive upper critical field $H_{c2}(T)$ using the value of temperature at 50% ρ_n is shown in the Fig. 7b. It is seen that both samples show a concave curvature (upward curvature) near T_{co} followed by a linear region which is in agreement with earlier studies [31]. The value of the upper critical field at absolute zero temperature, $H_{c2}(0)$ was estimated with a simplified WHH formula: $H_{c2}(0) = -0.693\ T^*\ (dH_{c2}/dT)_{T*}$ [32]. The slope is chosen to be the tangent to the curve $H_{c2}(T)$ near the highest field and T^* is at the intersection of this tangent with the temperature axis. The calculated $\mu_o H_{c2}(0)$ of the unmilled sample is around 240 T and it is highest (270 T) for the C-milled one. The higher H_{c2} corresponds to a stronger flux pinning potential. It is reported that the critical field shows the anisotropy characteristic of a quasi-two-dimensional superconductor, and it is highest when the field is oriented perpendicular to the c-axis. Previous $\mu_o H_{c2//}(0)$ measurements for magnetic field applied parallel to the c-axis of YBCO gave values varying from 56 to 120 T, however $\mu_o H_{c2\perp}(0)$ varies from 190 to 600 T when a field is applied perpendicular to the c-axis [33,34]. In our case the values of $\mu_o H_{c2}(0)$ are in the range of the $\mu_o H_{c2\perp}(0)$values and are larger than that reported in polycrystalline $Y(Ba_{1-x},Sr_x)_2Cu_3O_{7-d}$ (x=0.0–0.5) [31]. It seems that numerous CuO_2 planes in the crystallites are perpendicular to the applied magnetic field. Our estimated values seem reasonable in the context of bulk

Table 2
Zero resistance temperature T_{co} and critical current density of the milled and unmilled samples.

	Samples				
	A-milled	B-milled	C-milled	D-milled	Unmilled
T_{co} (K)	66	84.5	86.7	88.6	90
J_{ct} (A/cm^2)	–	32	115	158	160

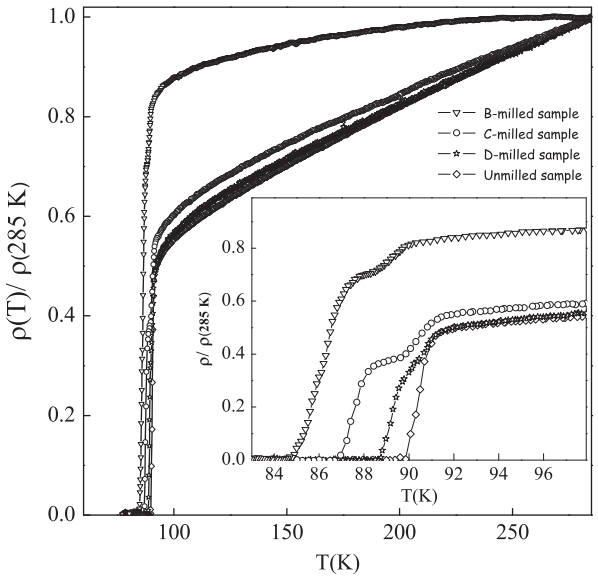

Fig. 5. Resistivity dependences on the temperature of the unmilled and milled samples. Inset: curves in the transition region for different samples.

polycrystalline samples. Because polycrystalline superconductors can be regarded as a distribution of YBCO crystallites with random orientation, thus at each orientation of the applied magnetic field$H_{c2}(0)$is most likely to be due to the combined contribution of $\mu_o H_{c2//}(0)$ and $\mu_o H_{c2\perp}(0)$.

The global transport critical current density of different samples was measured at 77 K in self magnetic field, J_{ct}, and the values are listed in Table 2. Note that different milling parameters, ball-to-powder weight ratio; rotation speed and the number of balls influence the critical current density. Note that the ball milling process reduces the J_{ct}. If we correlate the microstructure with the depression of J_{ct} in the milled samples, two possible arguments can be speculated; one, due to the degradation of the critical temperature and the second, more likely, would be due to the dispersion of finer grains in the superconducting matrix and as consequence the increase of the number of grain boundaries which brings more disorder in the sample. However, these J_{ct} values are interesting for all samples, especially when compared to the values reported in the literature in the case of $YBa_2Cu_3O_{7-d}$ doped with Ag nanoparticles [35] and $Y_{1-x}Ca_xBa_2Cu_3O_z$ [36] polycrystalline samples.

To isolate the flux pinning improvements, the measured $J_{ct}(H)$values in a magnetic fields can instead be normalized to the transport critical current density at zero-field values$J_{ct}(0)$. The dependences of the normalized transport critical current densities J_{ctN} on the magnetic field at various temperatures for all milled samples is shown in Fig. 8. J_{ctN} for unmilled sample was also plotted for comparison. All samples show a degradation of the normalized critical current density with increasing magnetic field. The deterioration of J_{ctN}due to the magnetic field is significantly reduced at low temperatures. The $J_{ctN}$of the B-milled sample declines sharply with magnetic field (Inset of Fig. 8). Moreover, J_{ctN} of the C-milled sample at 77 K is comparable to that of the unmilled sample, even its values at 40 and 20 K exceed those of the unmilled samples over the whole magnetic field in this study. The temperature dependences of the transport critical current density at applied magnetic field was also measured for both milled and unmilled samples; the measurements are shown in Fig. 9. Each of these samples shows an enhancement of the critical current with temperature ranging from near T_{co} down to $T = 20$ K. It is clear that the C-milled sample performances are better over the entire applied magnetic field ranges.

Fig. 10 shows the field dependence of the critical current density, $J_{cm}(H)$, determined from magnetic hysteresis loops at 77 K for C-milled and unmilled samples. The C-milled sample shows a much smoother decrease in $J_{cm}$with magnetic field. The obtained critical current densities ($J_{ct}(H)$ and $J_{cm}(H)$) were correlated with the microstructural features of the samples. Since the milled samples revealed a uniform distribution of nanosized inclusions, a higher density of flux pinning sites and an enhancement of critical current density can be expected. The attainment of optimum concentration and well-dispersed fine grains increases the number of grain boundaries and this would bring about more disorder and fine scale lattice defects. Both of these led to an increase of the flux pinning properties. However, surplus fine particles brought into the prepared milled sample might generate an excess of disorder in the superconducting matrix, which could result in the lower critical current density in the applied magnetic field.

To get more information about the pinning mechanism for milled and unmilled samples, it is customary to look for the scaling of the volume pinning force density F_p. The pinning force densities at 77 K are calculated as $F_p = \mu_o J_{cm} \times H$ from measurements of the magnetic critical current density. The scaled pinning reduced force $f_p = F_p/F_{pmax}$ often scales with $h = H/H_{max}$ instead of $h = H/H_{irr}$, where F_{pmax} is the maximum pinning force density, H_{max} is the field at which the $F_p$reaches its maximum and H_{irr} is the irreversible field. The scaling of $f_p$against h is often analyzed by using the following equations [37,38]:

for $\Delta\kappa$ pinning, $f_p = 3h^2(1-2h/3)$ (1)

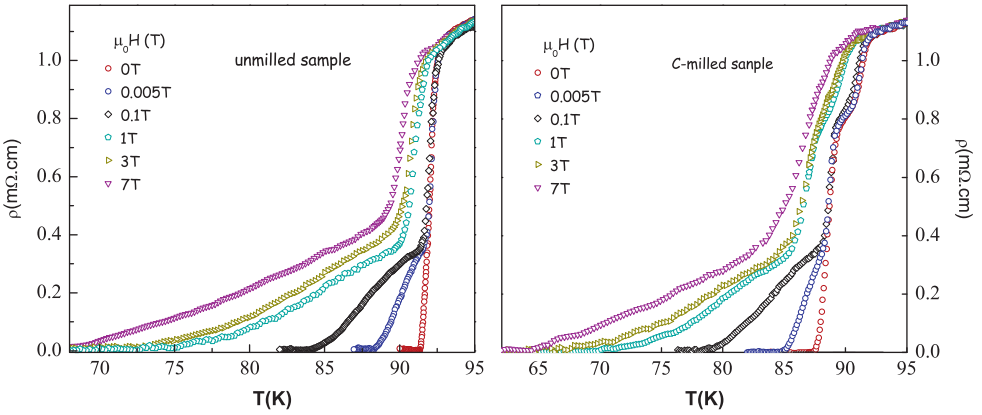

Fig. 6. Variations of the electrical resistivity with temperature at different applied magnetic fields of the unmilled and C-milled samples.

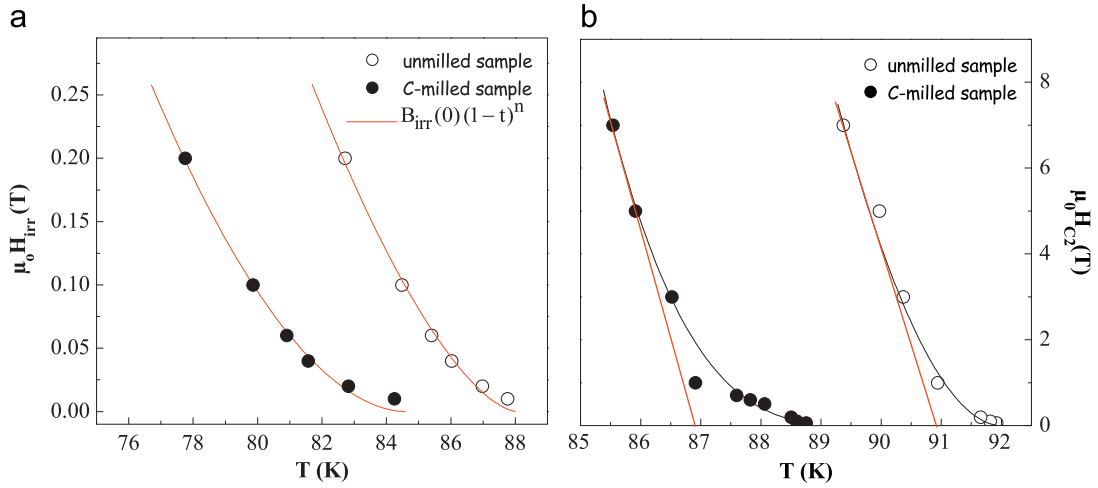

Fig. 7. Plots of the irreversibility magnetic field (a) and of the upper critical magnetic field (b) against the temperature (irreversibility line) for unmilled and C-milled samples.

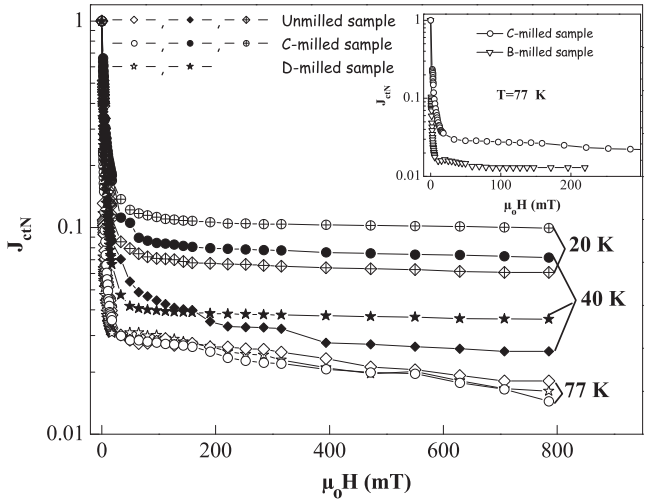

Fig. 8. Transport critical current density versus the magnetic field at various temperatures for the unmilled, C-milled and D-milled samples. Inset: J_{ct} versus applied magnetic field for the B-milled and C-milled samples at 77 K.

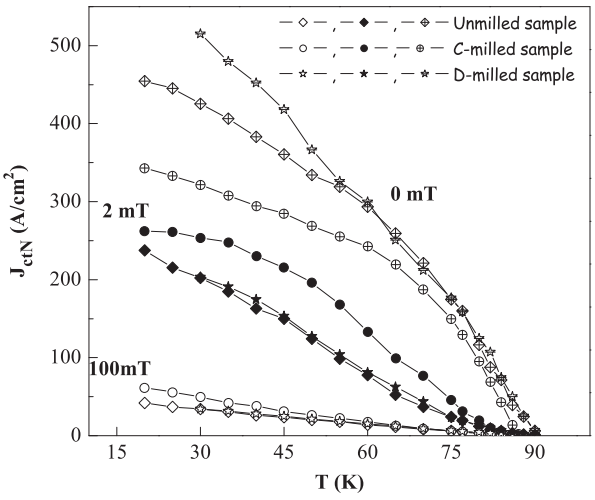

Fig. 9. Temperature dependence of the transport critical current density in various applied magnetic fields for the unmilled, C-milled and D-milled samples.

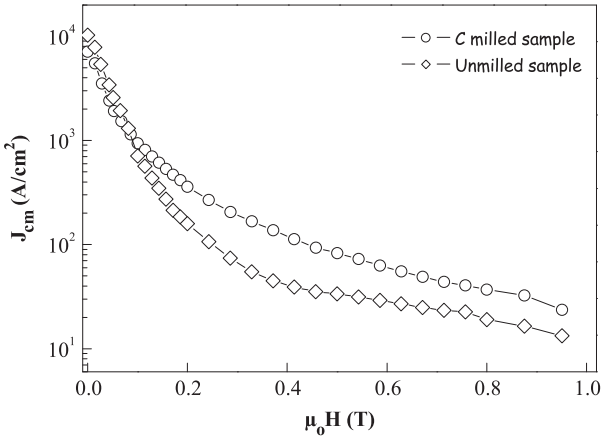

Fig. 10. Critical current density, calculated by magnetization loops versus magnetic fields at 77 K for the unmilled and C-milled samples.

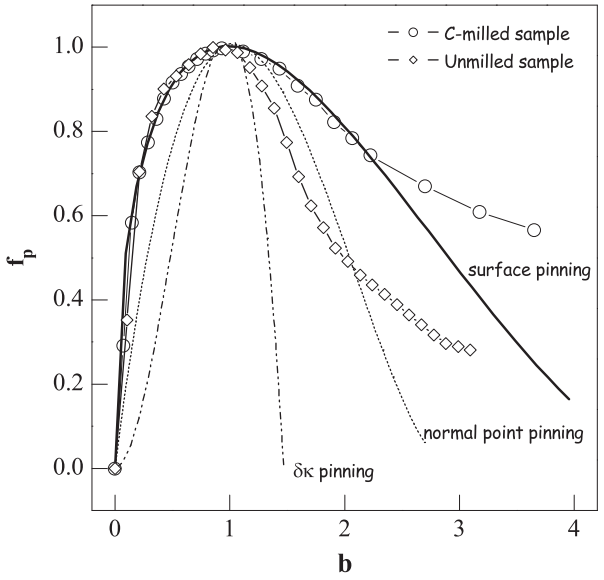

Fig. 11. Normalized pinning force against reduced magnetic fields at 77 K for the unmilled and C-milled samples. The continuous, dashed and dash-dot curves represent the fits based on Eqs. (1)–(3) of the text.

for normal point pinning, $f_p = 9/4\ h(1-h/3)^2$ (2)

and for surface pinning, $f_p = 25/16\ h^{1/2}(1-h/5)^2$ (3)

Fig. 11 shows the plots of the normalized pinning force f_p as a function of the reduced field, h at 77 K for C-milled and unmilled samples. For both samples, the large curves obtained indicate that the pinning properties cannot be explained by only one pinning mechanism over the whole region of the $f_p(h)$ curves. This implies that more than one type of pinning source may be present at the same time. A fitting procedure using Eqs. (1)–(3) was performed. For both samples in lower field regions, the $f_p(h)$ curves follow Eq. (3) which indicates that both samples almost completely accord with the surface pinning model. The contribution of surface pinning is higher in the C-milled sample than in the unmilled one, which results in an improvement of the f_p curve for a higher magnetic field of the milled sample. In higher field, for the milled sample the experimental points of the scaled pinning force are located above the surface pinning curves and this suggests the presence of strong pinning centers generated by the gathering of fine particles into coral-like agglomerates. Furthermore, the flux pinning force exceeds the prediction by the theoretical pinning model in higher fields.

We have used the ac-susceptibility,χ, measurements to determine the intergranular coupling. Fig. 12a and b shows the temperature dependence of the real,χ', and imaginary, χ'', components of the ac susceptibility curves measured at several magnetic field amplitudes and at a frequency $f = 10^3$ Hz. In polycrystalline HTS, a typical feature of χ is the appearance of two drops in χ' accompanied by two peaks inχ''. It is well known that if the applied field amplitude is large enough the temperature dependence of χ'' shows two peaks; one near T_c^{onset}associated with an intragranular critical current density and the second at a lower temperature correlated with the second drop in the real part χ' and related to the coupling matrix. The second peak is more affected by the external magnetic field because the intergranular pinning force is rather weak, while the intragranular peak is less sensible to the applied magnetic field because of the stronger pinning of vortices in the superconducting grains. The χ'' curves of our samples exhibit only one peak, indicating that these samples have no separation between the intragrain and the dissipative intergrain transition. This means that the applied magnetic field is not sufficient to penetrate the intragrain of the superconductor. Since the intragranular peak does not appear at the considered magnetic field, the intragranular pinning strength seems to be high in our samples. Fig. 12b shows that the intergranular loss peak shifts to lower temperature with an increase of the applied field. According to Bean's critical state model [23], this loss becomes maximum when the field reaches the center of the sample and the dependence of the intergrain critical current density as a function of peak temperature, T_P, of χ'' is written as: $J_{c\ int}(T_p) = H^*/\sqrt{ab}$ for a rectangular bar shaped sample of cross section $2a \times 2b$. The obtained intergranular critical current density, $J_{c\ int}$, is presented in Fig. 13. The temperature dependence of $J_{c\ int}$is found to obey the power law given by $J_{c\ int}(T) = J_{c\ int}(0)(1-T_p/T_{co})^n$ [39,40]. $J_{c\ int}(0)$ and 'n' were obtained from the best fit of the experimental data. The obtained value of n is equal to 1.7 and 1.5 respectively for unmilled and C-milled samples. This result indicates that both samples exhibit a similar Josephson junction type. The value of n between 1 and 2 is characteristic of superconductor–insulator–normal metal superconductor (SINS) junctions [41].

4. Conclusion

We considered the effects of a ball milling process on the superconducting properties of polycrystalline $YBa_2Cu_3O_y$ compounds. Samples were synthesized by the solid state reaction method by considering a thermal cycle with two stages of sintering at 950 °C separated by intermediate crushing; a traditional crushing (in a mortar) and another energetics (in a planetary crusher). We investigated the impact of the ball

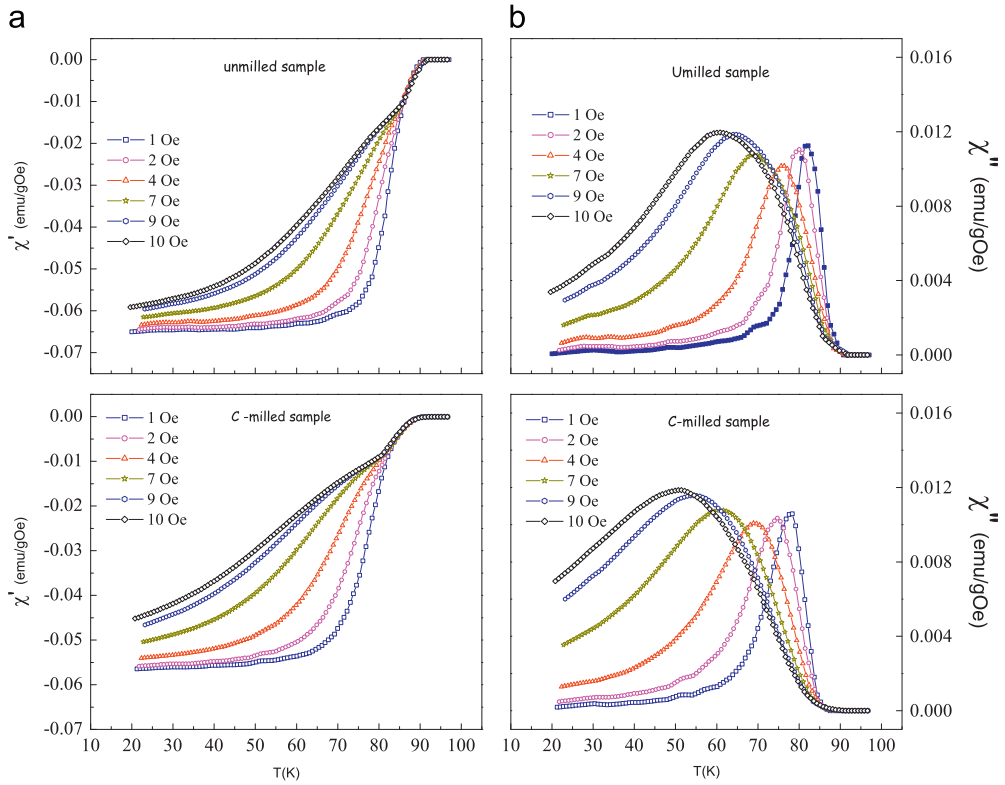

Fig. 12. Temperature dependence of the real component (a) and imaginary component (b) of *AC* susceptibility for the the unmilled and C-milled samples in the applied field ranging from 1 to 10 Oe with frequency of 1 kHz.

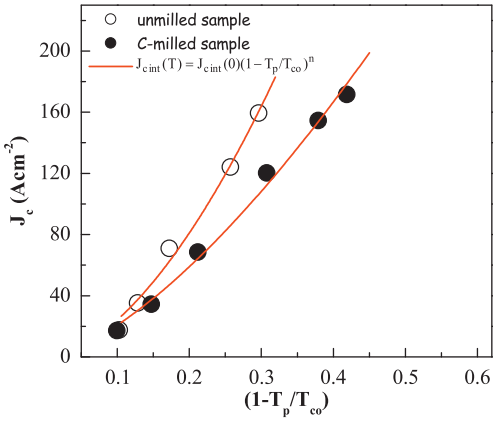

Fig. 13. Temperature dependence of the intergranular critical current density (symbols) and its fitting (solid line) using equation, $J_{c\ int} = J_{c\ int}(0)\ (1-T_p/T_{co})^n$ for the unmilled and C-milled samples.

milling parameters on the structure and microstructure of polycrystalline YBCO using XRD, SEM and EDXS. Current–voltage, ac-susceptibility and magnetization measurements were used in order to estimate the different critical currents densities. The correlation between microstructure development and superconducting properties has been elaborated. Ball-milled samples are composed of stoichiometric Y-123 and Y-deficient YBCO with a concentration varying with the milling parameters. The C-milled sample exhibits the better superconducting characteristics under an applied magnetic field. The global critical current density$J_{ct}(H)$, intra-grain critical current density $J_{cm}(H)$ and resistive upper critical H_{c2} and irreversibility H_{irr}magnetic fields have been improved for the C-milled sample. A high value of the upper critical field of 270 T was estimated for the C-milled sample by the WHH formula which is higher than for the unmilled one (240 T). SEM images show that the Y-deficient YBCO appears as a gathering of fine particles with a particle size around 10 nm into coral-like agglomerates embedded in the matrix. This finer structure contributes to the enhancement of the critical current density of the material under an applied magnetic field. The pinning force has been analyzed, and the results imply that the enhancement of the vortex flux pinning in the milled sample originates mainly from the surface pinning centers.

Acknowledgment

The authors are grateful to Prof G. Van Tendeloo (University of Antwerp Belgium) for useful discussions and text corrections.

References

[1] T. Matsushita, Flux pinning in superconducting 123 materials, Superconductor Science and Technology 13 (2000) 730.
[2] D. Larbalestier, A. Gurevich, D.M. Feldmann, A. Polyanski, High-Tc superconducting materials for electric power applications, Nature 414 (2001) 368.
[3] R. Goswami, T.J. Haugan, P.N. Barnes, G. Spanos, R.L. Holtz, Effects of nanoscale defects on critical current density of $(Y_{1-x}Eu_x)Ba_2Cu_3O_{7-\delta}$ thin films, Physica C 470 (2010) 318.

[4] F. Ben Azzouz, M. Zouaoui, A. Mellekh, M. Annabi, G. Van Tendeloo, M. Ben Salem, Flux pinning by Al-based nanoparticles embedded in YBCO: a transmission electron microscopic study, Physica C 455 (2007) 19.
[5] Y. Zhao, C.H. Cheng, J.S. Wang, Flux pinning by NiO-induced nano-pinning centres in melt-textured YBCO superconductor, Superconductor Science and Technology 18 (2005) S43.
[6] J. Plain, T. Puig, F. Sandiumenge, X. Obradors, J. Rabier, Microstructural influence on critical currents and irreversibility line in melt-textured $YBa_2Cu_3O_{7-x}$ reannealed at high oxygen pressure, Physical Review B 65 (2002) 104526.
[7] S.Y. Chen, I.G. Chen, Improvement to superconductivity using small amounts of Pd addition in Sm–Ba–Cu–O materials, Superconductor Science and Technology 17 (2004) 71.
[8] N.H. Babu, E.S. Reddy, D.A. Cardwell, A.M. Campbell, C.D. Tarrant, K.R. Schneider, Artificial flux pinning centers in large, single-grain (RE)-Ba–Cu–O superconductors, Applied Physics Letters 83 (2003) 4806.
[9] M. Miura, M. Mukaida, K. Matsumoto, Y. Yoshida, A. Ichinose, S. Horii, R. Kita, A. Saito, K. Kaneko, K. Yamada, N. Mori, Effects of $BaZrO_3$ dispersion into $EuBa_2Cu_3O_{7-\delta}$ superconducting thin films, Physica C 445 (2006) 845.
[10] K. Matsumoto, P. Mele, Artificial pinning center technology to enhance vortex pinning in YBCO coated conductors, Superconductor Science and Technology 23 (2010) 014001.
[11] N.M. Strickland, R.G. Buckley, A. Otto, High critical current densities in Cu-sheathed MgB_2 formed from a mechanically-alloyed precursor, Applied Physics Letters 83 (2003) 326.
[12] Y.F. Wu, Y.F. Lu, J.S. Li, S.K. Chen, G. Yan, M.H. Pu, C.S. Li, P.X. Zhang, The microstructures and superconducting properties of MgB_2 bulks prepared by a high-energy milling method, Physica C 467 (2007) 38.
[13] A. Gumbel, J. Eckert, G. Fuchs, K. Nenkov, K.-H. Muller, L. Schultz, Improved superconducting properties in nanocrystalline bulk MgB_2, Applied Physics Letters 80 (2002) 2725.
[14] J.H. Lee, S.Y. Shin, C.J. Kim, H.W. Park, Superconducting properties of MgB_2 prepared from attrition ball-milled boron powder, Journal of Alloys and Compounds 476 (2009) 919.
[15] Z. Ma, Y.C. Liu, J. Huo, Influence of ball-milled amorphous B powders on the sintering process and superconductive properties of MgB_2, Superconductor Science and Technology 22 (2009) 125006.
[16] X. Xu, J.H. Kim, S.X. Dou, S. Choi, J.H. Lee, H.W. Park, M. Rindfleish, M. Tomsic, A correlation between transport current density and grain connectivity in MgB_2/Fe wire made from ball-milled boron, Journal of Applied Physics 105 (2009) 103913.
[17] Z. Ma, Y. Liu, J. Huo, Z. Gao, MgB_2 superconductors with abnormally improved J_c sintered after autoxidation of milled original powders, Journal of Applied Physics 106 (2009) 113911.
[18] J.H Lee, B.H. Jun, C.J. Kim, H.W. Park, Effects of carbon substitution via ball-milling in MgB_2, Physica C 469 (2009) 1186.
[19] M. Simoneau, G. L'Esperance, M.L. Trudeau, R. Schulz, Structural and magnetic characterization of granular $Y_1Ba_2Cu_3O_{7-\delta}$ nanocrystalline powders, Journal of Materials Research 9 (1994) 535.
[20] J.Y. Xiang, C. Fleck, D.P. Hampshire, Bulk nanocrystalline superconducting $YBa_2Cu_3O_{7-x}$, Journal of Physics: Conference Series 97 (2008) 012237.
[21] A. Hamrita, F. Ben Azzouz, A. Madani, M. Ben Salem, Magnetoresistivity and microstructure of $YBa_2Cu_3O_y$ prepared using planetary ball milling, Physica C 472 (2012) 34.
[22] A. Hamrita, F. Ben Azzouz, W. Dachraoui, M. Ben Salem, The effect of silver inclusion on superconducting properties of $YBa_2Cu_3O_y$ prepared using planetary ball milling, Journal of Superconductivity and Novel Magnetism 26 (2013) 879.
[23] C.P. Bean, Magnetization of high-field superconductors, Physical Review Letters 8 (1962) 250.
[24] E.M. Gyorgy, R.B. van Dover, K.A. Jackson, L.F. Schneemeyer, J.V Waszczak, Anisotropic critical currents in $Ba_2YCu_3O_7$ analyzed using an extended Bean model, Applied Physics Letters 55 (1989) 283.
[25] A.H. Li, H.K. Liu, M. Ionescu, X.L. Wang, S.X. Dou, E.W. Collings, M.D. Sumption, M. Bhatia, Z.W. Lin, J.G. Zhu, Improvement of critical current density and thermally assisted individual vortex depinning in pulsed-laser-deposited $YBa_2Cu_3O_{7-\mathrm{delta}}$ thin films on $SrTiO_3$ (100) substrate with surface modification by Ag nanodots, Journal of Applied Physics 97 (2005) 10B107.
[26] R. Lortz, T. Tomita, Y Wang, A. Junod, J.S. Schilling, T. Masui, S. Tajima, On the origin of the double superconducting transition in overdoped $YBa_2Cu_3O_x$, Physica C 434 (2006) 194.
[27] A.I. Larkin, Yu.N. Ovchinnikov, Pinning in type II superconductors, Journal of Low Temperature Physics 34 (1979) 409.
[28] V.N. Vieira, P. Pureur, J. Schaf, Magnetic irreversibility limits of the Abrikosov and Josephson-flux dynamics in doped YBCO-123 superconductors, Physica C 354 (2001) 299.
[29] A.P. Malozemoff, T.K. Worthington, Y. Yeshurun, F. Holtzberg, P.H. Kes, Frequency dependence of the ac susceptibility in a Y–Ba–Cu–O crystal: a reinterpretation of H_{c2}, Physical Review B 38 (1988) 7203.
[30] B. Oh, K. Char, A.D. Kent, M. Naito, M.R. Beasley, T.H. Geballe, R. H. Hammond, A. Kapitulnik, J.M. Graybeal, Upper critical field, fluctuation conductivity and dimensionality of $YBa_2Cu_3O_{7-x}$, Physical Review B 37 (1988) 7861.
[31] N.P. Liyanawaduge, S.K. Singh, A. Kumar, R. Jha, B.S.B. Karunarathne, V.P.S. Awana, Magnetization and magneto resistance in $Y(Ba_{1-x}, Sr_x)_2Cu_3O_{7-d}$ ($x=0.00$–0.50) Superconductors, Superconductor Science and Technology 25 (2012)035017 25 (2012).
[32] N.R. Werthamer, E. Helfand, P.C. Hohenberg, Temperature and purity dependence of the superconducting critical field, h_{c2}. III. Electron spin and spin-orbit effects, Physical Review 147 (1966) 295.
[33] M.D. Lan, J.Z. Liu, Y.X. Jia, L. Zhang, Y. Nagata, P. Klavins, R.N. Shelton, Resistivity and upper critical field of $YBa_2Cu_{3-x}Fe_xO_{7-y}$ single crystals, Physical Review B 47 (1993) 457.
[34] Y. Hidaka, Y. Enomoto, M. Suzuki, M. Oda, A. Katsui, T. Murakami, Anisotropy of the upper critical magnetic field in single crystal $YBa_2Cu_3O_{7+y}$, Japan, Journal of Applied Physics 26 (1987) L726.
[35] M. Farbod, M.R. Batvandi, Doping effect of Ag nanoparticles on critical current of $YBa_2Cu_3O_{7-\delta}$ bulk superconductor, Physica C 471 (2011) 112.
[36] E.K. Nazarova, A.J. Zaleski, K.A. Nenkov, A.L. Zahariev, Intergranular flux pinning in underdoped and overdoped $R_{1-x}Ca_xBa_2Cu_3O_z$ ($R=Y$, Gd; $x=0$, 0.2) samples, Physica C 468 (2008) 955.
[37] T. Higuchi, S.I. Yoo, M. Murakami, Comparative study of critical current densities and flux pinning among a flux-grown $NdBa_2Cu_3O_y$ single crystal, melt-textured Nd–Ba–Cu–O, and Y–Ba–Cu–O bulks, Physical Review B 59 (1999) 1514.
[38] L. Klein, E.R. Yacoby, Y. Yeshurun, A. Erb, G. Müller, V. Breit, H. Wühl, Peak effect and scaling of irreversible properties in untwinned Y–Ba–Cu–O crystals, Physical Review B 49 (1994) 4403.
[39] V. Ambegaokar, A. Baratoff, Tunneling Between Superconductors, Physical Review Letters 10 (1963) 486.
[40] P.G. De Gennes, Boundary Effects in Superconductors, Reviews of Modern Physics 36 (1964) 225.
[41] H. Salamati, P. Kameli, Effect of deoxygenation on the weak-link behavior of $YBa_2Cu_3O_{7-\delta}$ superconductors, Solid State Communications 125 (2003) 407.